1998

A Nonisothermal Nickel-Hydrogen Cell Model

Pauline De Vidts
Texas A & M University - College Station

Javier Delgado

B. Wu

D. M. See
University of South Carolina - Columbia

K. Kosanovich

See next page for additional authors

Publication Info

Published in *Journal of the Electrochemical Society*, Volume 145, Issue 11, 1998, pages 3874-3883.

7. S. Motupally, M.S. Thesis, University of South Carolina, (1994).
8. A. Gorenstein, F. Decker, M. Fantini, and E. Estrada, *SPIE Inst. Adv. Opt. Tech.*, **IS 4**, 272 (1990).
9. P. Kofstad, *High Temperature Oxidation of Metals*, p. 53, John Wiley & Sons, Inc., New York (1966).
10. G. W. D. Briggs, *A Specialist Report: Electrochemistry*, Vol. 4, Burlington House, London (1974).
11. J. Scarminio, W. Estrada, A. Anderson, A. Gorenstein, and F. Decker, *J. Electrochem. Soc.*, **139**, 1236 (1992).
12. D. A. Corrigan and S. L. Knight, *J. Electrochem. Soc.*, **136**, 613 (1989).
13. G. W. D. Briggs and W. F. K. Wynne-Jones, *Electrochim. Acta*, **7**, 241 (1962)
14. G. W. D. Briggs, E. Jones, and W. F. K. Wynne-Jones, *Trans. Faraday Soc.*, **52**, 1433 (1956).
15. P. L. Bourgault and B. E. Conway, *Can. J. Chem.*, **38**, 1557 (1960).
16. P. L. Bourgault and B. E. Conway, *Can. J. Chem.*, **37**, 292 (1959).
17. B. Conway and E. Gileadi, *Can. J. Chem.*, **40**, 1933 (1962).
18. E. M. Kuchinskii and B. V. Erschler, *J. Phys. Chem., (U.S.S.R.)*, **14**, 985 (1940).
19. S. H. Glarum and J. H. Marshall, *J. Electrochem. Soc.*, **129**, 535 (1982).
20. C. Kittel, *Introduction to Solid State Physics*, 6th ed., pp. 567-569, John Wiley & Sons, Inc., New York (1986).
21. F. J. Morin, *Semiconductors*, pp. 616-629, John Wiley & Sons, Inc., New York (1959).
22. M. Abramowitz and I. A. Stegun, *Handbook of Mathematical Functions*, p. 299, Dover Publications, Inc., New York (1965).
23. K. P. Ta and J. Newman, *J. Electrochem. Soc.*, Submitted.
24. K. P. Ta, Ph.D. Thesis, University of California, Berkeley, LBNL-40353 (1997).
25. *Reference Electrodes*, D. J. Ives and G. J. Janz, Editors, Academic Press, Inc., New York (1961).
26. G. S. Atkinson, *Electrochem. Technol.*, **4**, 431 (1966).
27. D. F. Pickett, *J. Appl. Electrochem.*, **5**, 203 (1975).
28. H. Bode, K. Dehmelt, and J. Witte, *Electrochim. Acta*, **11**, 1079 (1966).
29. B. Paxton and J. Newman, *J. Electrochem. Soc.*, **144**, 3818 (1997).
30. C. Wagner, *J. Math. Phys.*, **34**, 289 (1954).
31. A. Acrivos and P. L. Chambré, *Ind. Eng. Chem. Fund.*, **49**, 1025 (1957).
32. P. D. Lukovtsev and G. J. Slaidin, *Electrochim. Acta*, **6**, 17 (1962).

A Nonisothermal Nickel–Hydrogen Cell Model

P. De Vidts,* J. Delgado, B. Wu, D. See, K. Kosanovich, and R. E. White***

Center for Electrochemical Engineering, Department of Chemical Engineering, University of South Carolina, Columbia, South Carolina 29208, USA

ABSTRACT

A previously presented mathematical model for a nickel–hydrogen cell has been extended to include thermal effects. A general energy balance, integral mass balances for the gases, and temperature-dependent parameters have been added to the model. Results for simulated isothermal and adiabatic conditions are shown. A comparison of simulation results to experimental data shows qualitative agreement.

Introduction

A sealed nickel–hydrogen cell is a hybrid electrochemical system combining electrode components of battery and fuel cell technologies. The nickel (positive) electrode was first developed for use in nickel-cadmium cells and the hydrogen (negative) electrode was originally used in hydrogen–oxygen fuel cells. Sealed nickel-hydrogen cells are designed to contain hydrogen gas under pressure within a cylindrical pressure cell as shown in Fig. 1. Inside the pressure vessel, there are a number of cell units connected in parallel to the outer leads (positive and negative terminals) of the cells. A cell unit is composed of one nickel electrode, a separator, a hydrogen electrode, and a gas screen. The model developed in this work applies to one or more cell units contained within a constant volume. A schematic diagram of a unit cell is shown in Fig. 2.

The positive electrode consists of a sintered porous nickel electrode which is electrochemically impregnated with nickel hydroxide active material. The negative electrode consists of a Teflon-bonded platinum black catalyst supported on a fine nickel mesh screen with a Teflon backing. The purpose of the Teflon backing is to prevent electrolyte loss through the back of the negative electrode while permitting free passage of hydrogen and oxygen gas. The gas screen placed behind the negative electrode consists of a mesh made of polypropylene fibers. The screen facilities transfer of hydrogen and oxygen gas from the head space of the cell pressure vessel to the back of the negative electrode. The pores of the cell components are wet with a concentrated potassium hydroxide solution. The pores are not flooded with electrolyte; part of the pore volume is occupied by a hydrogen and oxygen gas phase.

Thermal management is a critical factor in optimizing the performance of nickel-hydrogen batteries. At present, a great deal of effort is required to predict the rates of heat generation and removal for specific cell designs. Industrial models are frequently made by fitting semi-empirical equations to experimental observation collected from nickel–hydrogen cells.[1] This practice, while necessary for reliability in space applications, restricts the development of optimized cell designs because every proposed change must be built and tested, an expensive and time-consuming pro-

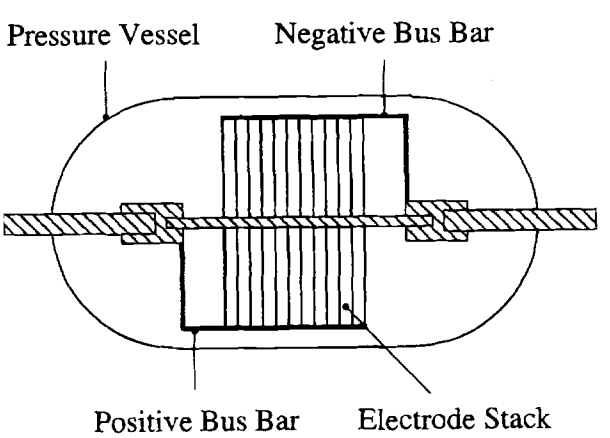

Fig. 1. Schematic diagram of the nickel–hydrogen cell modeled.

** Electrochemical Society Active Member.
* Electrochemical Society Student Member.

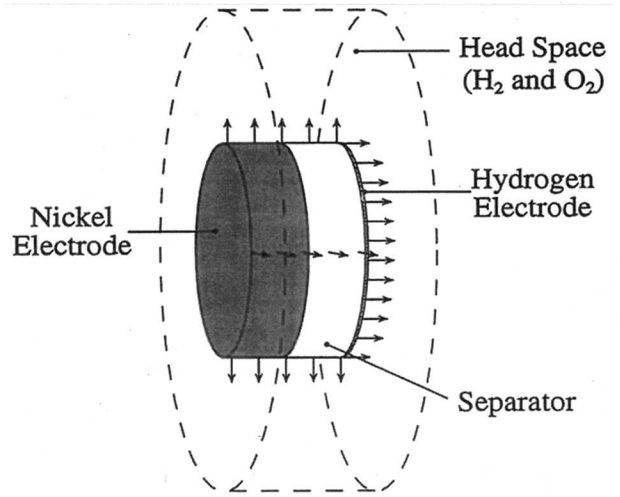

Fig. 2. Schematic diagram of a cell module in the nickel–hydrogen cell. Gas fluxes in the head space are shown.

cess. A detailed cell model which includes electrolyte composition profiles and current contribution fractions with an energy balance could be used as a development tool by researchers and battery engineers, reducing the need for experimental testing in the preliminary design process.

Kim et al.[2,3] dealt specifically with modeling the thermal characteristics of nickel–hydrogen cells. The primary purpose of their work was to model heat rejection and to optimize battery performance by minimizing water loss from the cell stack. As a result, these models calculate temperature gradients, but do not include detailed kinetics and mass transport within the modeled system. The multiphase isothermal model for a nickel–hydrogen cell, previously published by De Vidts et al.,[4] serves as the foundation for the work presented here. In the model, concentrated solution theory and the volume-averaging technique are used to characterize the transport phenomena of the electrolyte and gaseous species in a cell module. Proton diffusion through the active material on the nickel electrode is considered by including a pseudo-second-dimension in the nickel electrode with a simplified cylindrical geometry. Improvements to the theoretical model (as reported in this paper) include the addition of a general energy balance and temperature-dependent parameters. No temperature gradients within the cell are included; the cell is assumed to be isothermal at a particular instant in time as was done by Bernardi et al.[5]

Model

Assumptions.—The multiphase model of a nickel–hydrogen cell by De Vidts[6] showed that hydrogen and oxygen concentrations in the liquid and gas phases of the cell are essentially invariant with respect to the spatial direction. As a result, the mass balances of gas-phase and dissolved oxygen and hydrogen used by De Vidts have been simplified here by removing the spatial dependence. Temperature gradients in all spatial directions are neglected, and volumetric proportions of gas and liquid within the nickel electrode and separator are assumed to remain constant with time. It is assumed that no electrolyte passes through the platinum electrode, due to the Teflon backing. Also, it is assumed here that no water vapor exists in the vapor phase.

Governing equations.—A detailed derivation of the equations used in the multiphase model of a nickel–hydrogen cell has been presented earlier;[6,7] therefore, only the model equations that were changed or added as part of the thermal extension are presented in this paper. There are thirteen dependent variables. The dependent variables in the x direction are volume-averaged electrolyte concentration ($\langle c_e \rangle^l$), current density in the electrolyte (i^l), and potential (ϕ^l) in the electrolyte. The dependent variables in the y direction are proton concentration (c_{H^+}) and potential in the solid active material (ϕ^s). Figure 3 shows the system being modeled in the y direction, i.e., the pseudosecond dimension. The remaining variables ($c^{ext}_{H_2}$, $c^{ext}_{O_2}$, $c^{l}_{O_2}$, $c^{l}_{H_2}$, $c^{g}_{O_2}$, $c^{g}_{H_2}$, ϕ_{H_2}, and T) are functions of time only. The equations describing gas phase and dissolved gas mass transport in the electrolyte have been simplified by eliminating the spatial dependence and by assuming that the ideal gas law adequately describes the gas-phase behavior. Due to the high electrochemical driving force and low solubility of the gases in the electrolyte, one of the reactions has been modeled as being mass-transfer limited with a constant diffusion layer thickness. This reaction is the reduction of oxygen on the platinum electrode.

Electrochemical reactions.—Five electrochemical reactions are considered to occur within the cell unit. Three reactions occur within the porous nickel electrode: the main reaction, which involves the oxidation–reduction of nickel species within the active material, and two side reactions

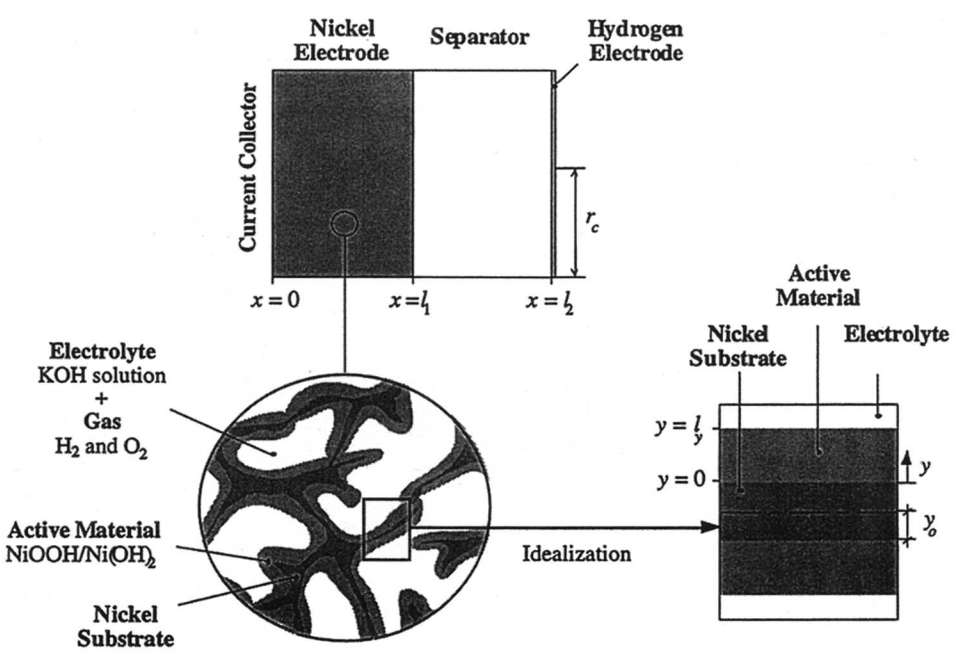

Fig. 3. Schematic diagram of the nickel–hydrogen cell showing the idealization of the nickel electrode and the coordinate system.

Nickel electrode main reaction

$$Ni(OH)_2 + OH^- \underset{\text{discharge}}{\overset{\text{charge}}{\rightleftharpoons}} NiOOH + H_2O + e^- \quad [1]$$

$$\text{side reaction 1} \quad 2\,OH^- \rightleftarrows \frac{1}{2}O_2 + H_2O + 2e^- \quad [2]$$

$$\text{side reaction 2} \quad \frac{1}{2}H_2 + OH^- \rightleftarrows H_2O + e^- \quad [3]$$

Two reactions occur on the platinum electrode: the primary reaction of water reduction–hydrogen oxidation and a side reaction

Hydrogen electrode main reaction

$$H_2O + e^- \underset{\text{discharge}}{\overset{\text{charge}}{\rightleftharpoons}} \frac{1}{2}H_2 + OH^- \quad [4]$$

$$\text{side reaction} \quad \frac{1}{2}O_2 + H_2O + 2e^- \rightarrow 2\,OH^- \quad [5]$$

As in the previous model by De Vidts et al.,[7] the electrochemical kinetics for reactions 1 through 4 are described by the Butler-Volmer equation, assuming stoichiometric reaction orders and a solvent activity of unity.[5,6] Assuming that Butler-Volmer kinetics apply, the temperature dependence of the exchange current density, $j_{o,k,\text{ref},T}$, may be expressed in the form of an Arrhenius expression[8]

$$j_{o,k,\text{ref},T} = j_{o,k,\text{ref},T_o} \exp\left[-\frac{\Delta E_k}{R}\left(\frac{1}{T} - \frac{1}{T_o}\right)\right] \quad [6]$$

In the following equations, the s, l, and g superscripts designate the solid, liquid, or gas phase, respectively.

For reaction 1 on the nickel electrode, the concentration-dependent kinetic expression describing the current is

$$j_1 = j_{o,1,\text{ref},T}\left\{\left(\frac{\langle c_e\rangle^l}{\langle c_{e,\text{ref}}\rangle^l}\right)\left(\frac{c_{H^+}}{c_{H^+,\text{ref}}}\right)_{y=l_y} \exp\left(\frac{\alpha_{a1}F}{RT}\eta_1\right) - \left(\frac{c_{H^+,\max} - c_{H^+}}{c_{H^+,\max} - c_{H^+,\text{ref}}}\right)_{y=l_y} \exp\left(\frac{-\alpha_{c1}F}{RT}\eta_1\right)\right\} \quad [7]$$

with the overpotential defined as

$$\eta_1 = \phi^s|_{y=l_y} - \phi^l - \phi_{1,\text{eq},\text{ref},T} \quad [8]$$

and with the equilibrium potential at the reference concentrations, given in the following intercalation form with respect to a Hg/HgO reference electrode and extended to account for temperature variation[9,10]

$$\phi_{1,\text{eq},\text{ref},T} = U_1^\theta - U_{RE}^\theta + (T - T_0)\left(\frac{dU_1}{dT} - \frac{dU_{RE}}{dT}\right) + \frac{RT}{F}\ln\left(\frac{c_{H^+,\text{ref}}}{c_{H^+,\max} - c_{H^+,\text{ref}}}\right) + \frac{RT}{F}k(2c_{H^+,\text{ref}} - 1) \quad [9]$$

For reaction 2 on the nickel electrode, the concentration-dependent kinetic expression is

$$j_2 = j_{o,2,\text{ref},T}\left\{\left(\frac{\langle c_e\rangle^l}{\langle c_{e,\text{ref}}\rangle^l}\right)^2 \exp\left(\frac{\alpha_{a2}F}{RT}\eta_2\right) - \left(\frac{c^l_{O_2}}{c^l_{O_2,\text{ref}}}\right)^{1/2} \exp\left(\frac{-\alpha_{c2}F}{RT}\eta_2\right)\right\} \quad [10]$$

with the overpotential defined as

$$\eta_2 = \phi^s|_{y=l_y} - \phi^l - \phi_{2,\text{eq},\text{ref},T} \quad [11]$$

and the equilibrium potential at reference concentrations described by

$$\phi_{2,\text{eq},\text{ref},T} = U_2^\theta - U_{RE}^\theta + (T - T_0)\left(\frac{dU_2}{dT} - \frac{dU_{RE}}{dT}\right) + \frac{RT}{F}\ln(p_{O_2,\text{ref}})^{1/2} \quad [12]$$

For reaction 3 on the nickel electrode, the concentration-dependent kinetic expression is

$$j_3 = j_{o,3,\text{ref},T}\left\{\left(\frac{\langle c_e\rangle^l}{\langle c_{e,\text{ref}}\rangle^l}\right)\left(\frac{c^l_{H_2}}{c^l_{H_2,\text{ref}}}\right)^{1/2} \exp\left(\frac{\alpha_{a3}F}{RT}\eta_3\right) - \exp\left(\frac{-\alpha_{c3}F}{RT}\eta_3\right)\right\} \quad [13]$$

with the overpotential defined as

$$\eta_3 = \phi^s|_{y=l_y} - \phi^l - \phi_{3,\text{eq},\text{ref},T} \quad [14]$$

and the equilibrium potential at reference concentrations described by

$$\phi_{3,\text{eq},\text{ref},T} = U_3^\theta - U_{RE}^\theta + (T - T_0)\left(\frac{dU_3}{dT} - \frac{dU_{RE}}{dT}\right) - \frac{RT}{F}\ln(p_{H_2,\text{ref}})^{1/2} \quad [15]$$

For reaction 4 on the hydrogen electrode, the concentration-dependent kinetic expression is

$$j_4 = j_{o,4,\text{ref},T}\left\{\left(\frac{\langle c_e\rangle^l}{\langle c_{e,\text{ref}}\rangle^l}\right)\left(\frac{c^l_{H_2}}{c^l_{H_2,\text{ref}}}\right)^{1/2} \exp\left(\frac{\alpha_{a4}F}{RT}\eta_4\right) - \exp\left(\frac{-\alpha_{c4}F}{RT}\eta_4\right)\right\} \quad [16]$$

with the overpotential defined as

$$\eta_4 = \phi_{H_2} - \phi^l|_{x=l_2} - \phi_{4,\text{eq},\text{ref},T} \quad [17]$$

and the equilibrium potential at reference concentrations described by

$$\phi_{4,\text{eq},\text{ref},T} = U_4^\theta - U_{RE}^\theta + (T - T_0)\left(\frac{dU_4}{dT} - \frac{dU_{RE}}{dT}\right) - \frac{RT}{F}\ln(p_{H_2,\text{ref}})^{1/2} \quad [18]$$

For reaction 5 on the hydrogen electrode, the current contribution made by oxygen reduction on the hydrogen electrode is assumed to be mass-transfer limited. Neglecting ion transference and assuming a constant Nernst diffusion layer, the following expressions can be written for the limiting current density and the limiting current density at a reference concentration[11]

$$j_5 = -\frac{n_5 F D_{O_2} c^l_{O_2}}{\delta} \quad [19]$$

$$j_{5,\text{ref},T} = -\frac{n_5 F D_{O_2} c^l_{O_2,\text{ref}}}{\delta} \quad [20]$$

Division of Eq. 19 by Eq. 20 results in the following expression used in the model

$$j_5 = j_{5,\text{ref},T}\frac{c^l_{O_2}}{c^l_{O_2,\text{ref}}} \quad [21]$$

The temperature dependence of the current density is again given by an Arrhenius expression

$$j_{5,\text{ref},T} = j_{5,\text{ref},T_0} \exp\left[-\frac{\Delta E_5}{R}\left(\frac{1}{T} - \frac{1}{T_0}\right)\right] \quad [22]$$

Cell module.—Within the cell module, the following mass-balance equations apply

Material balance of dissolved hydrogen

$$(\epsilon^{l}_{pos}l_1 + \epsilon^{l}_{sep}(l_2 - l_1))\frac{dc^{l}_{H_2}}{dt} = -\frac{a^{sl}_{pos}}{F}\int_0^{l_1} j_3 dx - \frac{a^{sl}_{neg}}{F}\int_{l_2}^{l_3} j_4 dx - a^{lg}_{pos}l_1 k^{lg}_{H_2}\left(\frac{c^{l}_{H_2}}{K_{e,H_2}} - c^{g}_{H_2}\right) - a^{lg}_{sep}(l_2 - l_1)k^{lg}_{H_2}\left(\frac{c^{l}_{H_2}}{K_{e,H_2}} - c^{g}_{H_2}\right) - k^{lg,ext}_{H_2}\left(\frac{c^{l}_{H_2}}{K_{e,H_2}} - c^{ext}_{H_2}\right) \quad [23]$$

Material balance of dissolved oxygen

$$(\epsilon^{l}_{pos}l_1 + \epsilon^{l}_{sep}(l_2 - l_1))\frac{dc^{l}_{O_2}}{dt} = \frac{a^{sl}_{pos}}{2F}\int_0^{l_1} j_2 dx + \frac{a^{sl}_{neg}}{2F}\int_{l_2}^{l_3} j_5 dx - a^{lg}_{pos}l_1 k^{lg}_{O_2}\left(\frac{c^{l}_{O_2}}{K_{e,O_2}} - c^{g}_{O_2}\right) - a^{lg}_{sep}(l_2 - l_1)k^{lg}_{O_2}\left(\frac{c^{l}_{O_2}}{K_{e,O_2}} - c^{g}_{O_2}\right) - k^{lg,ext}_{O_2}\left(\frac{c^{l}_{O_2}}{K_{e,O_2}} - c^{ext}_{O_2}\right) \quad [24]$$

Material balance of hydrogen in the gas phase inside the cell stack

$$(\epsilon^{g}_{pos}l_1 + \epsilon^{g}_{sep}(l_2 - l_1))\frac{dc^{g}_{H_2}}{dt} = a^{lg}_{pos}l_1 k^{lg}_{H_2}\left(\frac{c^{l}_{H_2}}{K_{e,H_2}} - c^{g}_{H_2}\right) + a^{lg}_{sep}(l_2 - l_1)k^{lg}_{H_2}\left(\frac{c^{l}_{H_2}}{K_{e,H_2}} - c^{g}_{H_2}\right) - \frac{2}{r_c}l_1 k^{ext}_{pos}RT\left(c^{g}_{H_2} - c^{ext}_{H_2}\right) - \frac{2}{r_c}(l_2 - l_1)k^{ext}_{sep}RT(c^{g}_{H_2} - c^{ext}_{H_2}) - k^{ref}_{tef}RT(c^{g}_{H_2} - c^{ext}_{H_2}) \quad [25]$$

Material balance of oxygen in the gas phase inside the cell stack

$$(\epsilon^{g}_{pos}l_1 + \epsilon^{g}_{sep}(l_2 - l_1))\frac{dc^{g}_{O_2}}{dt} = a^{lg}_{pos}l_1 k^{lg}_{O_2}\left(\frac{c^{l}_{O_2}}{K_{e,O_2}} - c^{g}_{O_2}\right) + a^{lg}_{sep}(l_2 - l_1)k^{lg}_{O_2}\left(\frac{c^{l}_{O_2}}{K_{e,O_2}} - c^{g}_{O_2}\right) - \frac{2}{r_c}l_1 k^{ext}_{pos}RT\left(c^{g}_{O_2} - c^{ext}_{O_2}\right) - \frac{2}{r_c}(l_2 - l_1)k^{ext}_{sep}RT(c^{g}_{O_2} - c^{ext}_{O_2}) - k^{ref}_{tef}RT(c^{g}_{O_2} - c^{ext}_{O_2}) \quad [26]$$

Gas pressure in the cell module pores and the head space.—The gaseous components within the modeled cell are assumed to behave as ideal gases and are described using the ideal gas equation as shown in Eq. 27 and Eq. 28.

Pressure in the gas pores

$$P^{int} = (c^{g}_{H_2} + c^{g}_{O_2})RT \quad [27]$$

Pressure in the head space

$$P^{ext} = (c^{ext}_{H_2} + c^{ext}_{O_2})RT \quad [28]$$

Thermal equations.—The equations used to describe the thermal behavior of the nickel–hydrogen cell include an energy balance and supporting equations. The cell energy balance considers the energy put in or removed from the cell, the changes in internal energy due to the electrochemical reactions, the pressure work, and the heat transfer to the outside of the pressure vessel. The derivation of the energy balance is presented in Appendix A

Cell energy balance

$$m_{cell}C_{p,cell}\frac{dT}{dt} = -hA_{vessel}(T - T_a) - i_{cell}(\phi_{sub} - \phi_{H_2}) - \sum_{k=1,2,3} N_{module}a^{sl}_{pos}A_{electrode}\int_0^{l_1} j_k dx\left(U_{k,avg} - T\left(\frac{dU_{k,avg}}{dT}\right)_p\right) - \sum_{k=4,5} N_{module}a^{sl}_{neg}A_{electrode}\int_{l_2}^{l_3} j_k dx\left(U_{k,avg} - T\left(\frac{dU_{k,avg}}{dT}\right)_p\right) + \left[V^{ext}\left(\frac{dP^{ext}}{dt}\right) + V^{int}\left(\frac{dP^{int}}{dt}\right)\right] \quad [29]$$

where the electrode are is

$$A_{electrode} = \pi r_c^2 \quad [30]$$

Mass of the cell

$$m_{cell} = N_{module}\pi r_c^2[\rho_{pos}l_1 + \rho_{sep}(l_2 - l_1) + \rho_{neg}(l_3 - l_2)] \quad [31]$$

Heat capacity of the cell

$$C_{p,cell} = \frac{N_{module}\pi r_c^2}{m_{cell}}[C_{p,pos}\rho_{pos}l_1 + C_{p,sep}\rho_{sep}(l_2 - l_1) + C_{p,neg}\rho_{neg}(l_3 - l_2)] \quad [32]$$

The above expression for the mass and heat capacity of the cell have neglected for simplicity the other components of the cell. The heat capacities and densities of the separator and nickel electrode in the equations above are calculated by considering the materials involved, including the porous volume occupied by gas and liquid phases. As a first approximation, density and heat capacity are considered to be independent of temperature over typical cell operating ranges.

Density of the positive electrode containing electrolyte

$$\rho_{pos} = \rho_{Ni}(1 - \epsilon_{o,pos}) + \rho_{Ni(OH)_2}(\epsilon_{o,pos} - \epsilon^{l}_{pos} - \epsilon^{g}_{pos}) + \rho_{KOH}\epsilon^{l}_{pos} \quad [33]$$

Density of the separator containing electrolyte

$$\rho_{sep} = \rho_{fiber}(1 - \epsilon^{l}_{sep} - \epsilon^{g}_{sep}) + \rho_{KOH}\epsilon^{l}_{sep} \quad [34]$$

Heat capacity of positive electrode containing electrolyte

$$C_{p,pos} = \frac{1}{\rho_{pos}}\left(C_{p,Ni}\rho_{Ni}(1 - \epsilon_{o,pos}) + C_{p,Ni(OH)_2}\rho_{Ni(OH)_2}(\epsilon_{o,pos} - \epsilon^{l}_{pos} - \epsilon^{g}_{pos}) + C_{p,KOH}\rho_{KOH}\epsilon^{l}_{pos}\right) \quad [35]$$

Heat capacity of separator containing electrolyte

$$C_{p,sep} = \frac{1}{\rho_{sep}}(C_{p,fiber}\rho_{fiber}(1 - \epsilon^{l}_{sep} - \epsilon^{g}_{sep}) + C_{p,KOH}\rho_{KOH}\epsilon^{l}_{sep}) \quad [36]$$

The electrolyte properties of gas solubility, thermodynamic activity, and diffusivity are given by the following equations.

Concerning the solubility of hydrogen and oxygen in the electrolyte, the Henry's law coefficient for dissolved hydrogen gas in potassium hydroxide is given as a function of concentration and temperature by the following empirical correlations obtained from Kimble[12]

$$K_{H_2} = \frac{1 - x_{H_2}}{x_{H_2}RT(2\langle c_e\rangle^{l} + 1.0 \times 10^{-7})} \quad [37]$$

in which the mole fraction of hydrogen gas, x_{H_2}, is expressed as

$$x_{H_2} = \frac{\exp[-48.1611 + \frac{5528.45}{T} + 16.8893\ln(0.01\,T)]}{10^{\{\langle c_e\rangle^{l}\{129\}\}}} \quad [38]$$

Similarly, Henry's law coefficient for oxygen is[12]

$$K_{O_2} = \frac{1 - x_{O_2}}{x_{O_2}RT(2\langle c_e\rangle^{l} + 1.0 \times 10^{-7})} \quad [39]$$

with the mole fraction of oxygen gas, x_{O_2}, expressed as

$$x_{O_2} = \frac{\exp[4.1741 + \frac{1.3104}{T} + \frac{3.417}{T^2} - \frac{2.4749}{T^3}]}{10^{\{\langle c_e\rangle^{l}(192.3 - 0.17T)\}}} \quad [40]$$

The electrolyte diffusion coefficient is represented as a function of concentration and temperature by fitting the following empirical equation (in a form suggested by Umino and Newman[13]) to available experimental data[14]

$$D_e = \exp\begin{pmatrix} -16.489 + 0.02015\,T - 8.1607[\langle c_e\rangle^1]^{0.5} + 286.2\langle c_e\rangle^1 \\ -2539.8[\langle c_e\rangle^1]^{1.5} + 7207.5[\langle c_e\rangle^1]^2 \end{pmatrix} \quad [41]$$

The molal activity coefficient of the electrolyte is given by the following empirical expression which was fit to experimental data from Akerlof and Bender[15]

$$\gamma_\pm = k_1 \exp(k_2) \quad [42]$$

and in which

$$k_1 = \frac{1}{(-56\langle c_e\rangle^1 + 1.0002 + 45.726\langle c_e\rangle^1 - 601.63[\langle c_e\rangle^1]^2)} \quad [43]$$

and

$$k_2 = 10^3\,\langle c_e\rangle^1(0.06629 + 6.135\times10^{-4}\,T - 1.1018\times10^{-5}\,T^2 + 4.096\times10^{-8}\,T^3)k_1 + 10^6[\langle c_e\rangle^1]^2(0.010909 - 1.7108\times10^{-4}\,T + 1.6895\times10^{-6}\,T^2 - 7.969\times10^{-9}\,T^3)k_1^2 + 10^9[\langle c_e\rangle^1]^3(-7.351\times10^{-4} + 9.973\times10^{-6}\,T - 9.347\times10^{-8}\,T^2 + 6.215\times10^{-10}\,T^3)k_1^3 + 10^{12}[\langle c_e\rangle^1]^4(1.5502\times10^{-5} - 1.98\times10^{-7}\,T + 1.8424\times10^{-9}\,T^2 - 1.764\times10^{-11}\,T^3)k_1^4 + 31.6228[\langle c_e\rangle^1]^{0.5}(0.48742 + 5.4567\times10^{-4}\,T + 7.9888\times10^{-6}\,T^2)/(1 + 44.7214c_e^{0.5}k_1) \quad [44]$$

Results and Discussion

The model formulated in the previous section was used to simulate cell performance during charge, open-circuit, and discharge processes at isothermal, adiabatic, and intermediate rates of heat transfer. General physical properties of the modeled cell and the model parameters used in the simulations are given in Table I. Some electrochemical parameters could not be found in the literature; hence, some fitted values were used. A simple trial-and-error procedure was used in the fitting. By changing the parameters of the model, it is found that the model predictions are most sensitive to the following parameters: α_{ak}, α_{ck}, ΔE_k, and j_{o,k,ref,T_0}. For anodic and cathodic transfer numbers α_{ak} and α_{ck}, the values in the literature have been used. The activation energy, ΔE_k, of each reaction was estimated. Since the charge and discharge voltage curves (except for the overcharge period) of the nickel-hydrogen cell show little sensitivity with respect to temperature, the activation energies of the main reactions, i.e., the nickel reaction and hydrogen reaction, will be small values. The activation energy and the reaction rate for oxygen evolution in the nickel electrode have great effects on the cell overcharge behavior, which can be calculated from the overcharge plateau in the experimental cell voltage curves at different temperatures. The reaction rates of other reactions were optimized by trial-and-error procedures.

The modeled cell (Fig. 1) consists of many cell modules (Fig. 2 and 3). The capacity of the modeled cell is the sum of that of the cell modules. The calculation of theoretical capacity of the cell is presented in Appendix B. The applied current on the cell was assumed to be evenly distributed among the cell modules. The charge and discharge rates used in the simulation are chosen based on the rated capacity of the cell.

Isothermal behavior at differing temperatures.—Under isothermal conditions, it is assumed that the cell remains at a uniform temperature unaffected by the heat generated inside the cell. Isothermal simulations were made by giving h, the heat transfer coefficient between the cell and its surroundings in the energy balance, a sufficiently high value to maintain a constant temperature in the cell. For these simulations, a heat transfer coefficient of 100 W/cm^2 K was used. The simulation consisted of a 3 A charge for 16 h, an open-circuit stand for 1 h, and a 15 A discharge to 0.0 V.

Table I. Model parameters used in the simulations.

Parameter	Values	Source
Kinetic		
$j_{o,1,ref,T_0}$	5.2×10^{-5} A/cm^2	a
$j_{o,2,ref,T_0}$	9.0×10^{-10} A/cm^2	a
$j_{o,3,ref,T_0}$	1.0×10^{-20} A/cm^2	a
$j_{o,4,ref,T_0}$	5.9×10^{-5} A/cm^2	a
j_{5,ref,T_0}	1.0×10^{-4} A/cm^2	a
$p_{H_2,ref}$	1.0 atm	
$p_{O_2,ref}$	1.0 atm	
T_0	293.15 K	
Thermodynamic		
ΔE_1	20×10^3 J/mol	b
ΔE_2	100×10^3 J/mol	b
ΔE_3	75×10^3 J/mol	b
ΔE_4	10×10^3 J/mol	b
ΔE_5	25×10^3 J/mol	b
k	0.3	a
U^θ_{RE}	0.0983 V	Ref. 10
U^θ_1	0.513 V	a
U^θ_2	0.4011 V	Ref. 10
U^θ_3	−0.8280 V	Ref. 10
U^θ_4	−0.8280 V	Ref. 10
U^θ_5	0.4011 V	Ref. 10
dU_{RE}/dT	-1.125×10^{-3} V/K	Ref. 10
dU_1/dT	-1.0×10^{-3} V/K	a
dU_2/dT	-1.6816×10^{-3} V/K	Ref. 10
dU_3/dT	-0.836×10^{-3} V/K	Ref. 10
dU_4/dT	-0.836×10^{-3} V/K	Ref. 10
dU_5/dT	-1.6816×10^{-3} V/K	Ref. 10
Cell		
A_{vessel}	1000.0 cm^2	
$A_{electrode}$	50.0 cm^2	
C	30 Ah	
$C_{p,Ni}$	0.46 J/g K	
$C_{p,Ni(OH)_2}$	0.46 J/g/ K	
$C_{p,KOH}$	3.14 J/g K	
$C_{p,fiber}$	1.67 J/g K	
$C_{p,neg}$	1.88 J/g K	
N_{module}	24	
r_c	3.99 cm	
V^{ext}	450.0 cm^3	
V^{int}	10.0 cm^3	
δ	3.5×10^{-4} cm	
ρ_{Ni}	8.9 g/cm^3	
$\rho_{Ni(OH)_2}$	3.4 g/cm^3	
ρ_{KOH}	1.29 g/cm^3	
ρ_{fiber}	0.91 g/cm^3	
ρ_{neg}	1.707 g/cm^3	
Initial conditions for charge		
$\langle c_e\rangle^1$	5.8×10^{-3} mol/cm^3	
c_{H^+}	0.99 $c_{H^+,max}$	
$p^0_{H_2}$	1.0×10^{-2} atm	
$p^0_{O_2}$	1.0×10^{-5} atm	

The parameters that have no source listed are either assumed values or design parameters. Other parameters can be found in Ref. 4. The parameters with source[a] are fitted values. The parameters with source[b] are estimated values.

The simulated cell voltages at three temperatures are shown in Fig. 4. As temperature increases, the cell voltage during the charge period decreases, which is due to the faster reaction rates at the higher temperatures (less polarization is needed). A similar trend has been observed in published (nonisothermal) experimental data.[12] The second voltage plateau during the charging process corresponds to cell overcharging. In the overcharge period, the main reactions in the cell are oxygen evolution in the nickel electrode and oxygen reduction at the platinum electrode. Since the oxygen evolution rate in the nickel electrode is slow, high polarization is needed to maintain the charge rate. At high temperature, the oxygen evolution rate will be fast enough to compete with the nickel main reaction, and the overcharge plateau becomes less pronounced. The cell discharge capacity is less at higher temperatures because the charging efficiency is low due to the competition of the oxygen reactions.

Figure 5 shows the variation in cell pressure for the isothermal simulations. In all cases, during the overcharge

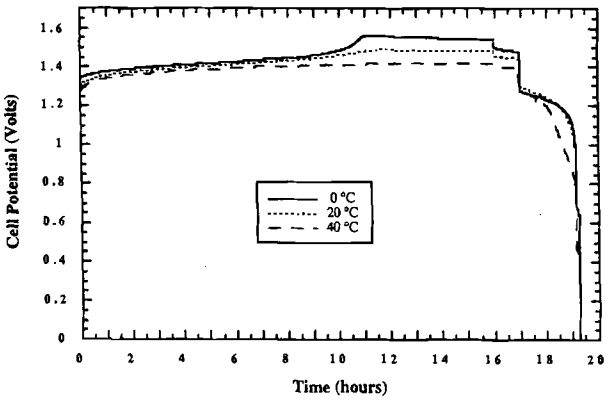

Fig. 4. Simulated isothermal voltage curves for a 3 A charge for 16 h, an open-circuit stand for 1 h, and a 15 A discharge to 0.0 V at 0, 20, and 40°C.

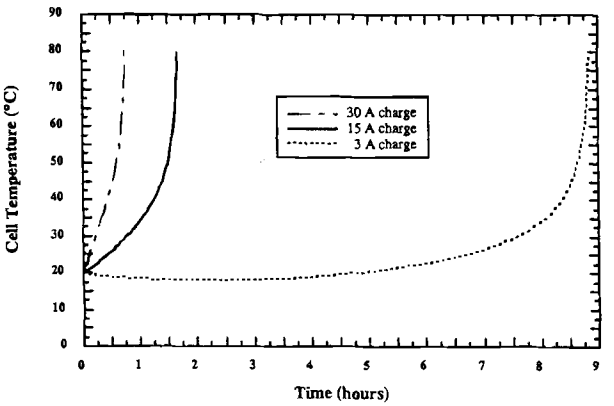

Fig. 6. Simulated temperature profiles for adiabatic charge simulations at charge rates of 3, 15, and 30 A.

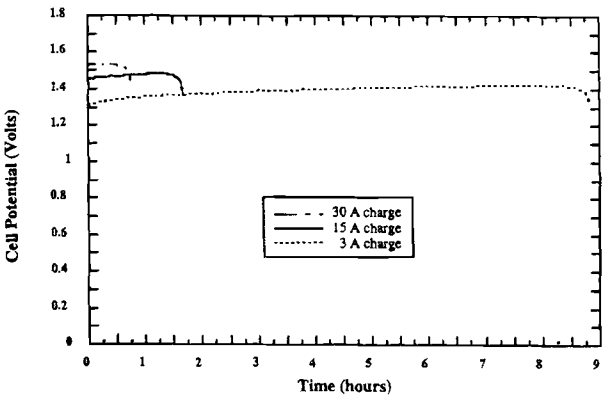

Fig. 7. Simulated voltage profiles for adiabatic charge simulations at charge rates of 3, 15, and 30 A.

period, the change in pressure with time becomes nonlinear. The maximum pressure achieved during the isothermal charge process decreases with increasing temperature.

Adiabatic behavior at different charge–discharge conditions.—Under adiabatic conditions, there is no heat transfer between the cell and its surroundings (h, the heat transfer coefficient, has a value of zero), and the cell temperature will vary according to the internal heat generated. For clarity, separate charge and discharge processes were simulated. All processes were started from a cell temperature of 20°C and were terminated at a temperature of 80°C. Simulations were run for cell charging rates of 3, 15, and 30 A. All adiabatic discharge simulations were started from identical initial conditions; specifically, the cells were isothermally charged at a 3 A rate for 16 h at 20°C prior to discharge. Simulations were run for cell discharging rates of 3, 15, and 30 A.

Figure 6 shows the variation of the cell temperature with time for the three different charging rates. At the lowest charge rate, 3 A, the cell temperature slightly decreases, indicating that an endothermic reaction is dominating for part of the charging process. The primary reaction on the nickel electrode, the oxidation of Ni(II) to Ni(III) in the active material, is known to be endothermic. As this reaction slows, exothermic reactions and resistive heating rapidly increase the cell temperature. At higher charge rates, the resistive heating effects dominate, and the temperature continually increases within the cell.

Figure 7 shows the corresponding variation in voltage with time. Under adiabatic conditions, the cell voltage quickly reaches its maximum value and maintains it before abruptly decreasing when the temperature rapidly increases. Adiabatic pressure effects are shown in Fig. 8. In comparison to the isothermal simulations, the rate of change of the pressure with time increases as the overcharge reactions begin to take effect, instead of approaching a constant pressure value.

Figures 9-11 show the temperature, voltage, and pressure variations during adiabatic discharge. From Fig. 9, note that the temperature profiles are more linear than for the charging processes and that the cutoff temperature is reached in less than an hour for all three rates. The discharge voltage plateaus (Fig. 10) are approximately constant during the simulation. Under adiabatic discharge conditions, the cell pressure (Fig. 11) does not decrease in the linear fashion observed during isothermal discharge and, in fact, increases for the 3 A discharge rate.

Comparison with experimental data.—TRW contributed experimental cell acceptance data for nineteen 30 Ah

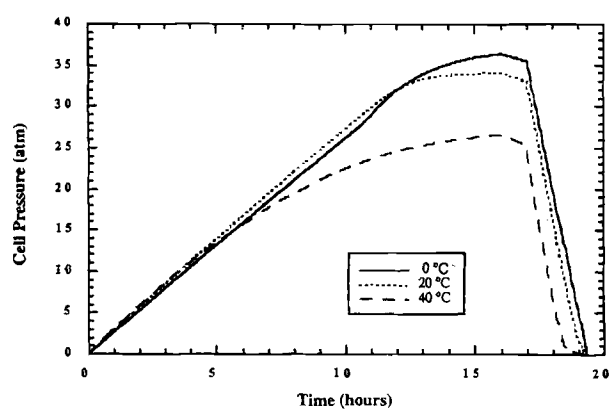

Fig. 5. Simulated isothermal pressure curves for a 3 A charge for 16 h, an open-circuit stand for 1 h, and a 15 A discharge to 0.0 V at 0, 20, 40°C.

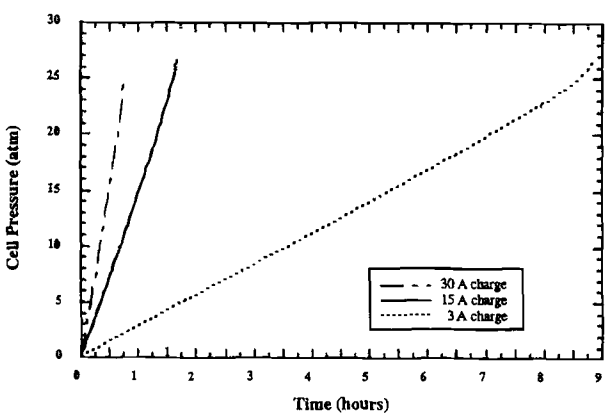

Fig. 8. Simulated pressure profiles for adiabatic charge simulations at charge rates of 3, 15, 30 A.

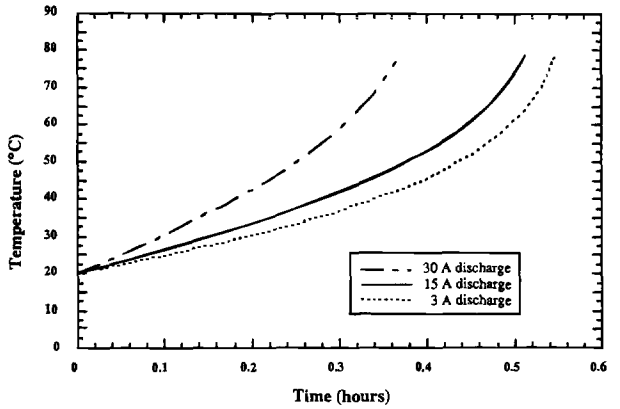

Fig. 9. Simulated temperature profiles for adiabatic discharge simulations at discharge rates of 3, 15, 30 A.

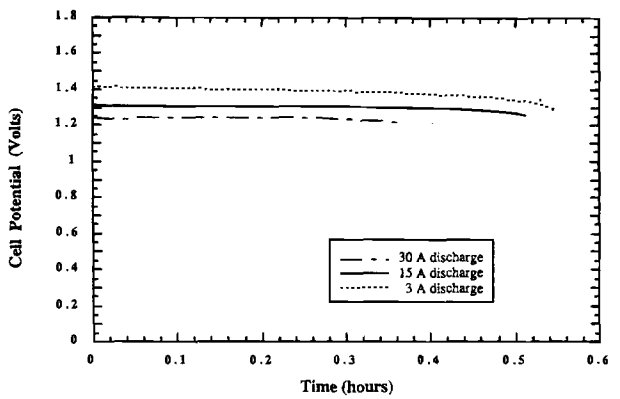

Fig. 10. Simulated voltage profiles for adiabatic discharge simulations at discharge rates of 3, 15, 30 A.

cells.[1] Their testing regime consists, in part, of a 3 A charge for 16 h, a stand of 1 h, and a 15 A discharge for 2.5 h. The experimental cells were placed in thermal sleeves and attached to a variable temperature heat sink. The heat sink temperature was controlled by thermistor readings at the top of the cells. The objective of the variable heat sink was to maintain the cell at its set-point temperature, in this case 20°C. A heat transfer coefficient of 5.0×10^{-3} W/cm^2 K is used in the simulation for comparison to the experimental data. This value was determined by fitting the simulation results to the average experimental temperature profile. The simulation discharge was terminated at a cutoff voltage of 0.0 V.

Figure 12 compares the average experimental voltage to the model predictions. There is excellent agreement between the experimental and simulated values over most of the testing period. The most significant variation occurs at the beginning of the charge cycle. The initialization process of the model predicts a higher starting voltage than the experimental value. In addition, there is a small difference in the experimental and simulated discharge capacities.

Figure 13 shows the average experimental and simulated temperature profiles. The simulation slightly underpredicts the temperature over the course of the test with the largest difference occurring during the discharge process. There is good qualitative agreement between the experimental data and simulated values. Figure 14 compares the average experimental pressure to simulated values. The experimental pressure data were normalized to 0 atm at the beginning of charge, since the strain gauges were reporting negative absolute pressure at the beginning of the

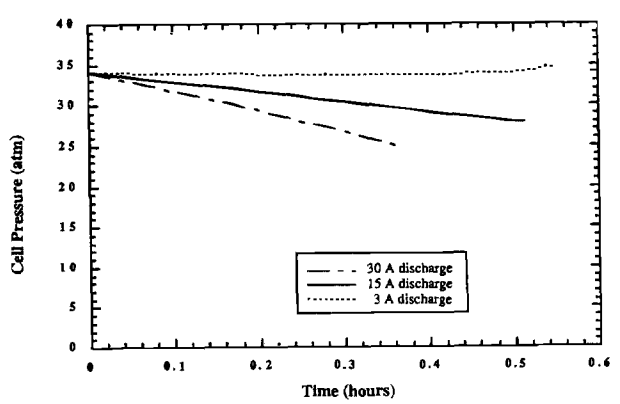

Fig. 11. Simulated pressure profiles for adiabatic discharge simulations at discharge rates of 3, 15, 30 A.

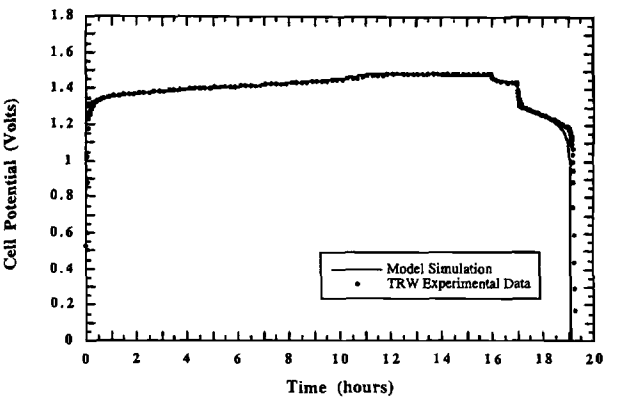

Fig. 12. Comparison of simulated cell voltage to experimental data.

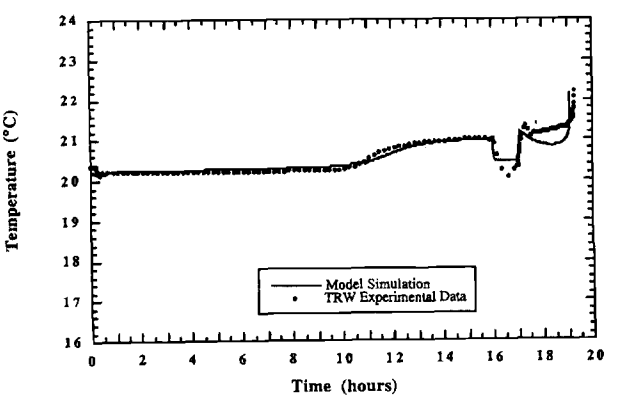

Fig. 13. Comparison of simulated cell temperature to experimental data.

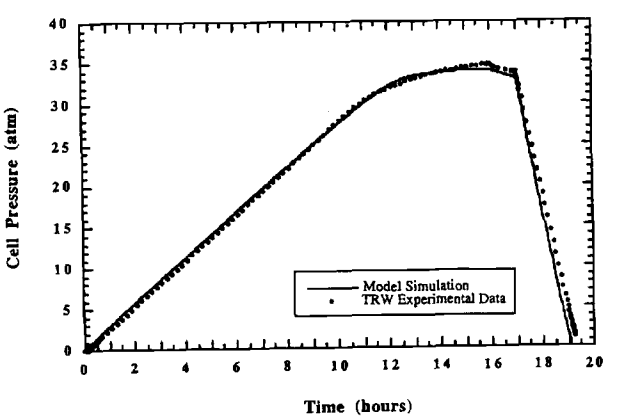

Fig. 14. Comparison of simulated cell pressure to experimental data.

charge process. There is good agreement between the experimental and simulated pressure curves.

Conclusions

A thermal extension of a nickel–hydrogen cell model is presented in this paper. The model may be used to evaluate the cell performance under various operating and design conditions for safety and preliminary design purposes. The performance results under isothermal and adiabatic conditions and an intermediate heat transfer rate are presented and analyzed. The model predictions are shown to be in good agreement with experimental data.

Acknowledgments

This work was supported by the Office of Research and Development of the United States Central Intelligence Agency. The authors gratefully acknowledge discussions with and experimental data from TRW engineers: Chuck Lurie, Bob Tobias, and Peter Loeff.

Manuscript submitted March 16, 1998; revised manuscript received August 5, 1998.

University of South Carolina assisted in meeting the publication costs of this article.

APPENDIX A

Energy Balance on the Cell Stack

Consider Fogler's[16] general transient energy balance for a chemical reactor

$$\dot{Q} - \dot{W}_s + \sum_{i=1}^{n} F_i H_i\big|_{in} - \sum_{i=1}^{n} F_i H_i\big|_{out} = \sum_{i=1}^{n} N_i \frac{dH_i}{dt} + \sum_{i=1}^{n} H_i \frac{dN_i}{dt} - \frac{d\left(P\sum_{i=1}^{n} N_i V_i\right)}{dt} \quad [A\text{-}1]$$

Some preliminary simplifications may be made to this general energy balance. Since the cell has no mass flowing in or out, the third and fourth terms may be removed from the left side of the equation. The pressure term may be expanded as follows

$$\frac{d\left(P\sum_{i=1}^{n} N_i V_i\right)}{dt} = \left[\left(\frac{dP}{dt}\right)\sum_{i=1}^{n} N_i V_i + P\frac{d}{dt}\left(\sum_{i=1}^{n} N_i V_i\right)\right] \quad [A\text{-}2]$$

In Eq. A-2

$$\sum_{i=1}^{n} N_i V_i = Vol_{cell} \quad [A\text{-}3]$$

Since the cell volume is constant, the second term on the right side of Eq. A-2 may be eliminated, yielding

$$\frac{d\left(P\sum_{i=1}^{n} N_i V_i\right)}{dt} = \left[\left(\frac{dP}{dt}\right)Vol_{cell}\right] \quad [A\text{-}4]$$

The heat flow in and out of the system, $\dot{Q}$, may be calculated using a heat-treatment coefficient

$$\dot{Q} = -hA_{vessel}(T - T_a) \quad [A\text{-}5]$$

The change in enthalpy with time may be restated in terms of heat capacity as follows

$$\sum_{i=1}^{n} N_i \frac{dH_i}{dt} = \sum_{i=1}^{n} m_i C_{p_i} \frac{dT}{dt} = m_{cell} C_{p,cell} \frac{dT}{dt} \quad [A\text{-}6]$$

When Eq. A-3 to A-6 are substituted into Eq. A-1, the general balance becomes the typical energy balance for a batch reactor

$$-hA_{vessel}(T - T_a) - \dot{W}_s = \sum_{i=1}^{n} m_i C_{p_i} \frac{dT}{dt} + \sum_{i=1}^{n} H_i \frac{dN_i}{dt} - \left[\left(\frac{dP}{dt}\right)Vol_{cell}\right] \quad [A\text{-}7]$$

Similar to Bernardi et al.,[5] the second term on the right side of Eq. A-7 can be approximated by

$$\sum_i H_i \frac{dN_i}{dt} = \int_v \sum_k a_k j_k \left(U_{k,avg} - T\left(\frac{dU_{k,avg}}{dT}\right)_P\right) dv \quad [A\text{-}8]$$

The electrical power is defined by

$$\dot{W}_s = i_{cell} V_{cell} \quad [A\text{-}9]$$

Incorporating equations Eq. A-8 and Eq. A-9 into Eq. A-7 yields an energy balance for an electrochemical batch reactor

$$m_{cell} C_{p,cell} \frac{dT}{dt} = -hA_{vessel}(T - T_a) - i_{cell} V_{cell} - \int_v \sum_k a_k j_k \left(U_{k,avg} - T\left(\frac{dU_{k,avg}}{dT}\right)_P\right) dv + \left[\left(\frac{dP}{dt}\right)Vol_{cell}\right] \quad [A\text{-}10]$$

V_{cell} is the potential difference between the nickel substrate and platinum electrode

$$V_{cell} = \phi_{sub} - \phi_{H_2} \quad [A\text{-}11]$$

The five reactions in the nickel-hydrogen cell can also be divided by where they happen. And finally, for convenience, Vol_{cell} may be divided into two parts: the gas volume within the stack, V^{int}, and the free volume of the cell, V^{ext}. The change in pressure may be similarly handled. The final energy balance is

$$m_{cell} C_{p,cell} \frac{dT}{dt} = -hA_{vessel}(T - T_{out}) - i_{cell}(\phi_{sub} - \phi_{H_2}) - \sum_{k=1,2,3} N_{module} a^{sl}_{pos} A_{electrode} \int_0^{l_1} j_k dx \left(U_{k,avg} - T\left(\frac{dU_{k,avg}}{dT}\right)_P\right) - \sum_{k=4,5} N_{module} a^{sl}_{neg} A_{electrode} \int_{l_2}^{l_3} j_k dx \left(U_{k,avg} - T\left(\frac{dU_{k,avg}}{dT}\right)_P\right) + \left[V^{ext}\left(\frac{dP^{ext}}{dt}\right) + V^{int}\left(\frac{dP^{int}}{dt}\right)\right] \quad [A\text{-}12]$$

APPENDIX B

Capacity of the Nickel–Hydrogen Cell

For a nickel–hydrogen cell, the theoretical capacity is determined by the following parameters: number of cell modules, area of the nickel electrode, thickness of the nickel electrode, porosity of the sintered nickel plaque, and loading of the nickel electrode

$$C = \frac{N_{module} A_{electrode} l_1 \epsilon_{o,pos} L_{Ni(OH)_2} F}{3600\ M_{Ni(OH)_2}} \quad [B\text{-}1]$$

However, the rated capacity of the nickel–hydrogen cell is determined by experiment, and some safety margin is always given. The rated capacity of a nickel–hydrogen cell is always lower than the theoretical value. The operation of the nickel–hydrogen cell is usually based on the rated cell capacity. For example, for a cell with a rated capacity of 30 Ah, a C/10 charge means a 3 A charge and a C/2 discharge means a 15 A discharge.

For a current, i_{cell}, on the nickel–hydrogen cell, the current density applied on the electrode, i_{app}, can be calculated by the following expression

$$i_{app} = \frac{i_{cell}}{N_{module} A_{electrode}} \quad [B\text{-}2]$$

For example, in Fig. 4, we have listed a 3 A charge for 16 h. This means that $i_{cell} = -3$ A during that period and

$$i_{app} = \frac{i_{cell}}{N_{module} A_{electrode}} = \frac{-3}{24 \times 50.0} = -2.5 \times 10^{-3} \text{ A/cm}^2 \quad [B\text{-}3]$$

This current density, $i_{app} = -2.5 \times 10^{-3}$ A/cm^2, is used as input for a unit-area model.

LIST OF SYMBOLS

A_{vessel} outside surface area of the cell pressure vessel, cm^2
$A_{electrode}$ projected electrode area of the cell module, cm^2
a_k surface area per unit volume of the porous electrode where reaction k occurs, cm^2/cm^3
a_{neg}^{sl} specific surface area of the solid/liquid interface (active area) per unit volume in the hydrogen electrode, cm^2/cm^3
a_{pos}^{lg} specific surface area of the liquid/gas interface per unit volume in the nickel electrode, cm^2/cm^3
a_{pos}^{sl} specific surface area of the solid/liquid interace per unit volume in the nickel electrode, cm^2/cm^3
a_{sep}^{lg} specific surface area of the liquid/gas interface per unit volume in the separator, cm^2/cm^3
$\langle c_e \rangle^l$ volume-averaged electrolyte concentration in the liquid phase, mol/cm^3
c_{H^+} proton concentration in the active material in the nickel electrode, mol/cm^3
$c_{H_2}^{ext}$ concentration of gaseous hydrogen in the head space, mol/cm^3
$c_{H_2}^{g}$ concentration of gaseous hydrogen in the gas phase of the cell stack, mol/cm^3
$c_{H_2}^{l}$ concentration of dissolved hydrogen in the liquid phase of the cell stack, mol/cm^3
$c_{O_2}^{ext}$ concentration of gaseous oxygen in the head space, mol/cm^3
$c_{O_2}^{g}$ concentration of gaseous oxygen in the gas phase of the cell stack, mol/cm^3
$c_{O_2}^{l}$ concentration of dissolved oxygen in the liquid phase of the cell stack, mol/cm^3
$C_{p,cell}$ heat capacity of the cell, J/g K
$C_{p,fiber}$ heat capacity of the solid phase of the separator, J/g K
$C_{p,KOH}$ heat capacity of the electrolyte, J/g K
$C_{p,neg}$ heat capacity of the negative (hydrogen) electrode and its contents, J/g K
$C_{p,Ni}$ heat capacity of the nickel substrate, J/g K
$C_{p,Ni(OH)_2}$ heat capacity of the active material in the nickel electrode, J/g K
$C_{p,pos}$ heat capacity of the positive (nickel) electrode and its contents, J/g K
$C_{p,sep}$ heat capacity of the separator and its contents, J/g K
dU_k/dT experimental temperature coefficient for the equilibrium potential of reaction k, V/K
$dU_{k,avg}/dT$ temperature coefficient for the equilibrium potential for reaction k at the average composition of reactants, which is approximated by a constant value dU_k/dT in this work, V/K
D_e diffusion coefficient of the electrolyte, cm^2/s
D_{H_2} diffusion coefficient of the dissolved hydrogen in the electrolyte, cm^2/s
D_{O_2} diffusion coefficient of the dissolved oxygen in the electrolyte, cm^2/s
F Faraday's constant, 96,487 C/equiv
F_i molar flow rate of species i, mol/s
h heat transfer coefficient between the cell and its surroundings, W/cm^2 K
H_i enthalpy of species i at temperature T, J/mol
i_{cell} current applied to the cell unit, A
i_{app} current density applied ot the electrode in the cell module, A/cm^2
j_k local current density due to reaction k taking place at the solid/liquid interface, A/cm^2
$j_{k,ref,T}$ reaction rate of reaction k at reference concentrations and temperature T expressed in the unit of currently density, A/cm^2
$j_{o,k,ref,T}$ exchange current density for reaction k at reference concentrations and temperature T, A/cm^2
k intercalation constant used in Eq. 9, dimensionless
k_1 empirical expression used in the activity coefficient expression, dimensionless
k_2 empirical expression used in the activity coefficient expression, dimensionless
K_{e,H_2} equilibrium constant for hydrogen, relating the concentration of hydrogen in the liquid and gas phases (Henry's law), dimensionless
K_{e,O_2} equilibrium constant for oxygen, relating the concentration of oxygen in the liquid and gas phases (Henry's law), dimensionless
$k_{H_2}^{lg}$ rate constant for the molar flux of hydrogen between the liquid and gas phases in the pores of the cell components, cm/s
$k_{H_2}^{lg,ext}$ rate constant for the molar flux of hydrogen between the liquid at the back of the hydrogen electrode and the gas phase right outside the back of the hydrogen electrode, cm/s
$k_{O_2}^{lg}$ rate constant for the molar flux of oxygen between the liquid and gas phases in the pores of the cell components, cm/s
$k_{O_2}^{lg,ext}$ rate constant for the molar flux of oxygen between the liquid at the back of the hydrogen electrode and the gas phase right outside the back of the hydrogen electrode, cm/s
k_{pos}^{ext} rate constant for the molar flux of gas species between the internal and external gas phases at the positive electrode, mol/atm cm^2 s
k_{sep}^{ext} rate constant for the molar flux of gas species between the internal and external gas phases at the separator, mol/atm cm^2 s
k_{tef}^{ext} rate constant for the molar flux of gas species between the internal and external gas phases at the back of the hydrogen electrode, mol/atm cm^2 s
l_1 x coordinate for the location of the interface between the nickel electrode and the separator (thickness of nickel electrode), cm
l_2 x coordinate for the location of the interface between the separator and the hydrogen electrode, cm
l_3 x coordinate for the location of the back of the hydrogen electrode, cm
l_y thickness of the active material layer in the nickel electrode, cm
$L_{Ni(OH)_2}$ loading of active material in the porous nickel electrode active material, g/cm^3 void volume
m_{cell} mass of the cell, g
$M_{Ni(OH)_2}$ molecular weight of $Ni(OH)_2$, g/mol
n number of electrons involved in a specific reaction, equiv
n_k number of electrons involved in reaction k
N_i number of moles of species i, mol
N_{module} number of cell modules in the nickel-hydrogen cell
P system pressure in the energy balance equation, Pa
P^{ext} total pressure of gas in the head space, atm
$p_{H_2,ref}$ reference pressure of hydrogen, atm
P^{int} total pressure of gas in the gas phase of the cell stack, atm
$p_{O_2,ref}$ reference pressure of oxygen, atm
Q heat flow from the surroundings to the system, J/s
R universal gas constant, 8.3143 J/mol K
r_c cell stack radius, cm
t time, s
T temperature, K
T_a ambient temperature outside the cell, K
T_0 reference temperature, 298.15 K
$U_{k,avg}$ theoretical open-circuit potential for reaction k at the average composition of reactants (averaged across the electrode for a one dimensional porous electrode model) relative to a reference electrode of a given kind, V
U_k^0 standard cell potential for reaction k, V
ν volume integration symbol, cm^3
V_{cell} cell voltage, V
V^{ext} volume of the head space between the cell stack and the pressure vessel (external gas space), cm^3
V_i partial molar volume of species i, cm^3/mol
V^{int} gas volume in the cell stack (internal gas space), cm^3
Vol_{cell} cell volume, cm^3
$\dot{W}_s$ work done by the system on the surroundings, J/s
x_{H_2} mole fraction of hydrogen gas, dimensionless
x_{O_2} mole fraction of oxygen gas, dimensionless

Greek

α_{ak} anodic transfer coefficient of reaction k, dimensionless

α_{ck}	cathodic transfer coefficient of reaction k, dimensionless
δ	diffusion layer thickness, cm
ΔE_k	activation energy for reaction k, J/mol
$\epsilon_{o,pos}$	porosity of the nickel substrate before impregnation of active material, dimensionless
ϵ^g_{pos}	gas porosity of the positive electrode, dimensionless
ϵ^l_{pos}	liquid porosity of the positive electrode, dimensionless
ϵ^g_{sep}	gas porosity of the separator, dimensionless
ϵ^l_{sep}	liquid porosity of the separator, dimensionless
ϕ_{H_2}	potential of the hydrogen electrode, *V*
$\phi_{k,eq}$	equilibrium potential for reaction k, *V*
$\phi_{k,eq,ref}$	equilibrium potential for reaction k at reference concentrations, *V*
ϕ_{sub}	potential in the nickel substrate of the nickel electrode, *V*
$\gamma_{\pm}$	mean molal activity coefficient of the solute in the electrolyte, dimensionless
ρ_{fiber}	mass density of the separator solid phase, g/cm^3
ρ_{KOH}	mass density of the electrolyte, g/cm^3
ρ_{neg}	mass density of the negative (hydrogen) electrode and its contents, g/cm^3
ρ_{Ni}	mass density of the nickel substrate of the nickel electrode, g/cm^3
$\rho_{Ni(OH)_2}$	mass density of the active material in the nickel electrode, g/cm^3
ρ_{pos}	mass density of the positive (nickel) electrode and its contents, g/cm^3

REFERENCES

1. C. Lurie, B. Tobias, and P. Loeff, TRW Space and Electronics Group, Personal communication.
2. J. Kim, T. V. Nguyen, and R. E. White, *J. Electrochem. Soc.*, **139,** 2781 (1992).
3. J. Kim, T. V. Nguyen, and R. E. White, *J. Electrochem. Soc.*, **141,** 333 (1994).
4. P. De Vidts, J. Delgado, and R. E. White, *J. Electrochem. Soc.*, **143,** 3223 (1996).
5. D. Bernardi, E. Pawlikowski, and J. Newman, *J. Electrochem. Soc.*, **132,** 5 (1985).
6. P. De Vidts, Ph.D. Thesis, Texas A & M University, College Park, TX (1995).
7. P. De Vidts and R. E. White, *J. Electrochem. Soc.*, **144,** 1343 (1997).
8. W. Schmickler, *Interfacial Electrochemistry,* Oxford University Press, New York (1996).
9. D. Fan and R. E. White, *J. Electrochem. Soc.*, **138,** 2952 (1991).
10. S. G. Bratsch, *J. Phys. Chem. Ref. Data,* **18,** 1 (1989).
11. A. Bard and D. Faulkner, *Electrochemical Methods: Fundamentals and Applications,* Wiley, New York (1980).
12. M. C. Kimble, Ph.D. Thesis, Texas A & M University, College Park, TX (1991).
13. S. Umino and J. Newman, *J. Electrochem. Soc.*, **140,** 2217 (1993).
14. V. Lobo and J. Quaresma, *Electrolyte Solutions: Literature Data on Thermodynamic and Transport Properties,* Vol. 2, Elsevier, New York (1981).
15. G. Akerlof and P. Bender, *J. Am. Chem. Soc.*, **70,** 2366 (1948).
16. H. S. Fogler, *Elements of Chemical Reaction Engineering,* 2nd ed., p. 425, Prentice-Hall, Englewood Cliffs, NJ (1994).